water

MDPI

Article

Variations of Surface and Subsurface Water Storage in the Lower Mekong Basin (Vietnam and Cambodia) from Multisatellite Observations

Binh Pham-Duc [1,2,3,*], Fabrice Papa [4,5], Catherine Prigent [2], Filipe Aires [2], Sylvain Biancamaria [4] and Frédéric Frappart [4]

1 Space and Aeronautics Department, University of Science and Technology of Hanoi, Vietnam Academy of Science and Technology, 18 Hoang Quoc Viet, Cau Giay, Hanoi 10000, Vietnam
2 LERMA, UMP 8112, l'Observatoire de Paris, 61 Avenue de l'Observatoire, 75014 Paris, France; catherine.prigent@obspm.fr (C.P.); filipe.aires@obspm.fr (F.A.)
3 Aix-Marseille Université, IRD, CEREGE, Europôle de l'Arbois, 13545 Aix-en-Provence, France
4 LEGOS, Université de Toulouse, IRD, CNES, CNRS, UPS, 31400 Toulouse, France; fabrice.papa@ird.fr (F.P.); sylvain.biancamaria@legos.obs-mip.fr (S.B.); frederic.frappart@legos.obs-mip.fr (F.F.)
5 IFCWS, Indo-French Cell for Water Sciences, IRD-IISc Joint International Laboratory, Indian Instutute of Science, Bangalore 560012, India
* Correspondence: pham@cerege.fr; Tel.: +33-7-8243-5237

Received: 31 October 2018; Accepted: 30 December 2018; Published: 4 January 2019

Abstract: In this study, we estimate monthly variations of surface-water storage (SWS) and subsurface water storage (SSWS, including groundwater and soil moisture) within the Lower Mekong Basin located in Vietnam and Cambodia during the 2003–2009 period. The approach is based on the combination of multisatellite observations using surface-water extent from MODIS atmospherically corrected land-surface imagery, and water-level variations from 45 virtual stations (VS) derived from ENVISAT altimetry measurements. Surface-water extent ranges from ~6500 to ~40,000 km^2 during low and high water stages, respectively. Across the study area, seasonal variations of water stages range from 8 m in the upstream parts to 1 m in the downstream regions. Annual variation of SWS is ~40 km^3 for the 2003–2009 period that contributes to 40–45% of total water-storage (TWS) variations derived from Gravity Recovery And Climate Experiment (GRACE) data. By removing the variations of SWS from GRACE-derived TWS, we can isolate the monthly variations of SSWS, and estimate its mean annual variations of ~50 km^3 (55–60% of the TWS). This study highlights the ability to combine multisatellite observations to monitor land-water storage and the variations of its different components at regional scale. The results of this study represent important information to improve the overall quality of regional hydrological models and to assess the impacts of human activities on the hydrological cycles.

Keywords: MODIS; satellite altimetry; Lower Mekong Basin; surface-water extent; surface-water volume; subsurface-water volume

1. Introduction

The Mekong River is one of the largest river systems in the world, covering ~4300 km in length and a drainage area of more than 800,000 km^2 [1]. The source of the Mekong River originates in the Himalayas before flowing through six countries (China, Myanmar, Laos, Thailand, Cambodia, and Vietnam), and entering the Eastern Sea in one of the largest worldwide deltas [1]. The Mekong Basin is commonly divided into two major parts: the Upper Mekong Basin (UMB), mostly located in China, and the Lower Mekong Basin (LMB), located in the other countries [1]. The overall map of

the Mekong River basin (with upper and lower basin boundaries and river network) and our study area in the LMB (black rectangle) are shown in Figure 1-left. The LMB, which is the main focus of the study, is home to more than 60 million people (∼35% of the total population of Laos, Thailand, Cambodia, and Vietnam [1]), and is one of the most important regions of Southeast Asia, economically and environmentally [2]. The LMB region includes the Tonle Sap Lake (also called the Great Lake) in Cambodia, the largest freshwater lake in Southeast Asia, and the Mekong Delta in Vietnam, a vast triangular plain of approximately 55,000 km^2, mainly located few meters above the sea. They are both very important for ecosystems (the lake is home to nearly 150 fish species, reptiles, and birds) and for local human activities and resources. For instance, the Mekong Delta region, which covers only 12% of Vietnam, produces 50% of annual rice and hosts 50% of fisheries and 70% of fruit production [3]. These regions are now seriously affected by climate change, sea-level rise, and anthropological pressure on water resources [4–6], exacerbated by fast annual growing populations (1–2%/year in Thailand and Vietnam, and 2–3%/year in Cambodia and Laos). For instance, the construction of dams for electricity production in the upper part of the Mekong basin in Laos and China has also caused large impacts on the LMB, such as recent changes in the magnitude and seasonality of water flows that impact the flood pulse of the Tonle Sap Lake and the Vietnamese Mekong Delta (VMD) [7]. The region is also vulnerable to extreme events, and the frequency of tropical storms has increased in La Nina years causing deadly and costly floods, while in El Nino years, such as 2014–2016, droughts lasted longer than usual, with serious consequences on the environment and the economy [8].

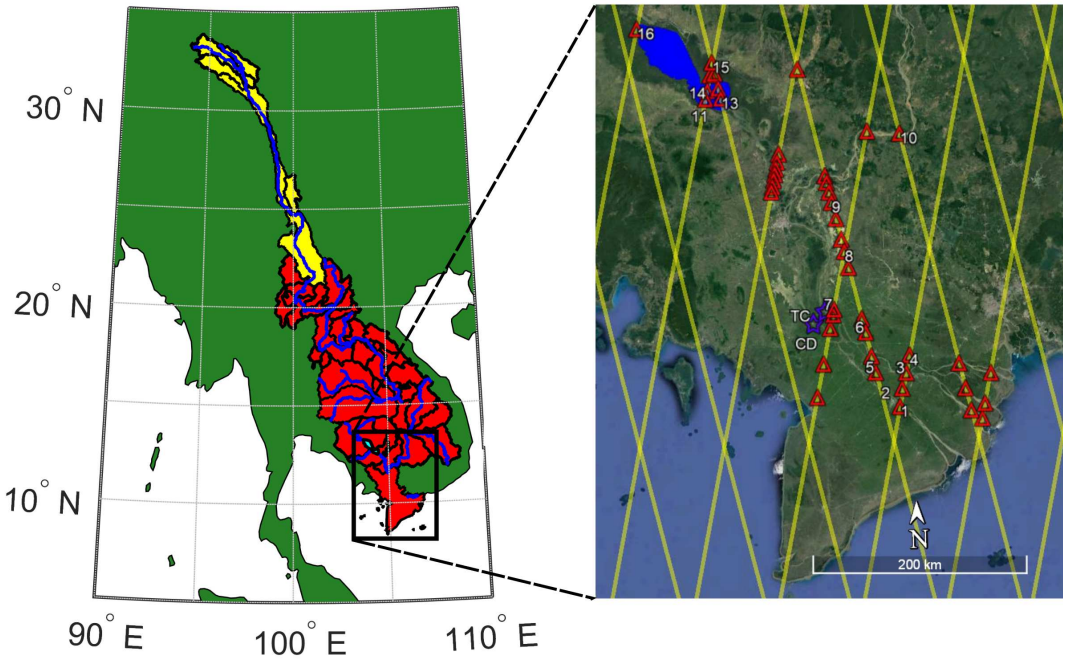

Figure 1. (**Left**) Upper and lower Mekong basins (yellow and red, respectively), and the Mekong River network (blue). The black rectangle shows our study area (Lower Mekong Basin located in Vietnam and Cambodia). (**Right**) Detailed map of the study area, where the yellow lines represent the ENVISAT satellite tracks, red triangles represent locations of ENVISAT virtual stations, and blue stars represent locations of the Tan Chau (TC) and Chau Doc (CD) gauge stations. The normal extent of the Tonle Sap Lake at a low water stage (blue) is also presented.

Similar to many of the world's major deltas, the Mekong has experienced significant anthropogenic changes during the past decades, including land-use change [9], mainly to develop agriculture dominated by rice paddies [10]. This resulted in widespread overexploitation of freshwater resources [11], with excessive groundwater usage during the last decades resulting in various problems, such as the rapid falling of groundwater levels [12]. In such areas, overabstraction of groundwater

resources can amplify natural subsidence processes [13]). In the VMD, new evidence of widespread absolute subsidence was revealed by Interferometric Synthetic Aperture Radar (InSAR) [14–16], which demonstrated that a steady increase of groundwater use and excessive pumping over the past decades has dramatically accelerated subsidence in this area. In this context, monitoring the variations of the different components of the hydrological cycle in the region, including surface-water extent, water level, and water storage (both surface and subsurface), is extremely important. In general, however, in situ observations in the LMB are very sparse and not available to the scientific community. With the development of satellite observations, many satellite-based products are now available over the LMB that allow us to widen our current knowledge on the variation of the water-cycle component of the region. However, our knowledge of the distribution and variations of water storage, especially groundwater storage in the LMB, is incomplete.

Since 2002, the Gravity Recovery And Climate Experiment (GRACE) provides, for the first time, precise measurements of spatiotemporal variations in the total terrestrial water storage or TWS (the sum of groundwater, soil water, surface water, and snow pack) [17] at seasonal and basin scales. Several studies have estimated subsurface water storage change (SSWS) from GRACE-derived TWS estimates [18–21] after deducting the contribution of changes in the other water-storage compartment, in particular, surface-water storage (SWS; see Reference [22] for a review). Recently, some authors have combined different multisatellite observations to quantify the variation of the surface-water extent and storage of several worldwide lakes, reservoirs, and basins [23–25]. Papa et al. (2015) [26] combined surface-water extent at 25 km spatial resolution from the Global Inundation Extent from Multisatellite (GIEMS [27–29]) and water-level height variations derived from ENVISAT altimetry data for the entire Ganges–Brahmaputra basin over the 2003–2007 period. This technique was first introduced in the Amazon and the Ob basins [18,30–32], proving that the approach combining satellite-based surface-water extent maps and altimetry data is powerful to monitor surface freshwater-storage changes at basin scale. Over LMB, monthly variation of the surface-water volume for the 1998–2003 period were estimated by combining surface-water extent maps derived from the Normalized Difference Vegetation Index (NDVI) of the SPOT-4 Vegetation instrument and ERS-2/ENVISAT altimetry data [33]. However, since GRACE data were not available for that period, it was impossible to estimate the variation of the subsurface-water storage over the LMB.

In the present study, our goal is to apply this multisatellite technique over the LMB located in Vietnam and Cambodia, to quantify the variations of the SWS and SSWS in the hydrological cycle, and estimate their contribution to TWS. To this end, surface-water extent maps derived from MODIS imagery at 500 m spatial resolution are combined with surface-water level variations maps estimated using ENVISAT altimetry data, similar to what was recently proposed by Frappart et al. (2018) [34] and Normandin et al. (2018) [35]. The study area was limited to latitude lower than the 13.5° (black rectangle in Figure 1–left) where ENVISAT altimetry data were good enough for extraction of surface-water height. At higher latitudes, the Mekong River is too steep and narrow, causing the loss of many data, as the altimeter tracking loop remained locked on the top of the hills (see Reference [36] for a detailed explanation). As a consequence, ENVISAT altimetry does not perform well over the river, with very noisy estimates, and it is impossible to properly extract the variations of water level of the Mekong River. The period 2003–2009 was chosen as it covers the years for which all datasets used in this study are overlapping in time.

Details of satellite and ancillary datasets used in this study are described in Section 2. In Section 3, the methodology to estimate the monthly variations of SWS and SSWS, including groundwater and soil moisture, for the 2003–2009 period, is presented. Results, comparisons, and discussions are presented in Section 4. Finally, conclusions and perspectives are drawn in Section 5.

2. Datasets

2.1. Satellite Datasets

2.1.1. Moderate Resolution Imaging Spectroradiometer (MODIS) Land-Surface Reflectance Satellite Observations

The MODIS instrument is one of the key instruments onboard the Terra satellite (launched on 18 December 1999), and the Aqua satellite (launched on 4 May 2002) from NASA. The two satellites are sun-synchronous, near-polar, and are orbiting at an altitude of ∼705 km. The satellites were designed so that the Terra satellite passes the equator from north to south at 10.30 a.m. (local time), and the Aqua satellite passes the equator from south to north at 1.30 p.m. (local time). They can cover Earth's entire surface every 1–2 days. In this study, atmospherically corrected land surface reflectance 8-Day Level 3 Global 500 m products from MODIS/Terra (MOD09A1) are used to create monthly surface water extent maps of the LMB at 500 m spatial resolution, for the 2003–2009 period. Each MOD09A1 image was created by selecting the best Level-2 gridded (L2G) observation during an eight-day period on the basis of high observation coverage, low view angle, absence of clouds or cloud shadow, and aerosol loading [37]. MODIS/Terra satellite observations are free to download from NASA's EarthData Hub (https://search.earthdata.nasa.gov/search).

2.1.2. ENVISAT Satellite Altimetry Data

The ENVISAT mission was launched on 1 March 2002 by the European Space Agency (ESA). It carried 10 instruments, including the advanced radar altimeter (RA-2). It was based on the heritage of the sensor on-board the ERS-1 and 2 satellites. It orbited at an average altitude of 790 km, with an inclination of 98.54°, on a sun-synchronous orbit with a 35-day repeat cycle. They provided observations of the Earth surface (ocean, land, and ice caps) from 82.4° latitude north to 82.4° latitude south. This orbit was formerly used by the ERS-1 and 2 missions, with an equatorial ground-track spacing of about 85 km. RA-2 was a nadir-looking pulse-limited radar altimeter operating at two frequencies at Ku- (13.575 GHz), as ERS-1 and 2, and S- (3.2 GHz) bands [38]. ENVISAT tracks over the LMB are shown in Figure 1-right, along with locations of 45 virtual stations (VS) used in this study for monitoring of the surface water height. A virtual station is defined as the intersection between the satellite ground tracks and a water surface [39]. ENVISAT remained on its nominal orbit until October 2010 and its mission ended on 8 April 2012, following the unexpected loss of contact with the satellite. RA-2 stopped operating correctly at the S-band in January 2008. Altimetry data used in this study were processed, validated, and distributed by the Center of Topography of Oceans and the Hydrosphere (CTOH) in the Laboratoire d'Études en Géophysique et Océanographie Spatiales (LEGOS), France (http://ctoh.legos.obs-mop.fr/).

2.2. Other Datasets

2.2.1. Total Water Storage from GRACE Data

GRACE data are used to estimate the total land surface-water storage, with an accuracy of ∼1.5 cm of equivalent water thickness [40,41]. GRACE spatial resolution is ∼300 km, but the product we downloaded is distributed on a 1°× 1° pixel-size grid. Calculation is based on measurements of the spatial–temporal change in the gravity field of Earth that results mainly from the redistribution of water mass in surface-fluid envelops [42]. Since its launch in March 2002, monthly GRACE gravity-solutions data are provided by three different processing centers: the GeoforschungsZentrum Potsdam (GFZ), the Center for Space Research at University of Texas, Austin (CSR), and the Jet Propulsion Laboratory (JPL). To reduce noise in the gravity-field solutions, the average of the three products is used in this study as suggested by Sakumura et al. (2014) [43]. Then, the average product was multiplied with the provided GRACE scaling factor to increase the accuracy of the GRACE total water-storage estimates,

as suggested in [44]. Monthly GRACE Level-3 (Release 05) Land-Mass Grids products and its scaling factor are available at https://grace.jpl.nasa.gov/data/get-data/monthly-mass-grids-land/.

2.2.2. Surface Water Storage from the WaterGap Global Hydrology Model

The WaterGAP Global Hydrology Model (WGHM) is a submodel of global water use that computes groundwater storage, total water storage, baseflow, groundwater recharge (diffuse and below surface water bodies at a spatial resolution of 0.5° [45,46]. WGHM is based on the best global datasets currently available. For comparison with our multisatellite-based results, outputs from the WaterGap 2.2a model are used to compute monthly variation of the land surface- and subsurface-water storage within the LMB (area shown in Figure 1-right). WGHM model outputs are available at https://www.uni-frankfurt.de/49903932/7_GWdepletion.

2.2.3. In Situ Water Level and Discharge Data

In situ water level and discharge information of the Mekong River at the Tan Chau (10.48° N, 105.13° E) and Chau Doc (10.42° N, 105.06° E) stations are collected for validation of our results. The sum of discharge at the two stations is almost equal to the total discharge of the Mekong River when it flows from Cambodia to Vietnam. In situ discharge data are provided by the Vietnam Southern Regional Hydrometeorological Center (VSRHC; http://www.kttv-nb.org.vn/).

3. Methodology

3.1. Land Surface-Water Extent Mapping

Monthly surface-water extent maps at 500 m spatial resolution of the study area can be constructed based on a methodology introduced by Sakamoto et al. (2007) [47] that was specifically designed and developed for tropical regions like the Mekong basin [3]. This methodology uses low values of water indices as main indicators for surface-water presence, and it has been used in previous studies over the LMB [3,5]. Here, we present a quick summary of the methodology. First, the Enhanced Vegetation Index (EVI), the Land Surface-Water Index (LSWI), and the Different Value between EVI and LSWI (DVEL) are calculated at pixel level, from the original atmospherically corrected surface reflectance data derived from the MOD09A1 eight-day composite products. The EVI and the LSWI are obtained using Equations (1) and (2), while the DVEL is calculated by Equation (3):

$$EVI = 2.5 * \frac{NIR - RED}{NIR + 6 * RED - 7.5 * BLUE + 1} \quad (1)$$

$$LSWI = \frac{NIR - MIR}{NIR + MIR} \quad (2)$$

$$DVEL = EVI - LSWI \quad (3)$$

where RED, NIR, BLUE, and MIR are the surface-reflectance values of Visible Band 1 (red; 620–670 nm), NIR Band 2 (841–876 nm), Visible Band 3 (blue; 459–479 nm), and MIR Band 6 (1628–1652 nm), respectively. Next, a linear interpolation is used to deal with missing data such as cloud-covered pixels (where surface-reflectance values of the blue band >= 0.2), then a simple weight-smoothing function is applied to smooth the indices [3]. For classification, all pixels with smoothed EVI values >= 0.3 are classified as nonflooded pixels. Water-related pixels are marked when the smoothed DVEL values <= 0.05 and the smoothed EVI values <= 0.3. If a pixel has its smoothed EVI value <= 0.05 and its smoothed LSWI value <= 0, it is also marked as a water-related pixel. At the final step, a threshold on the smoothed EVI values is used to distinguish between mixed pixels and fully inundated pixels from water-related pixels. Mixed pixels are defined as pixels that are partly inundated. The smoothed EVI values in open-water bodies, such as lakes or the ocean, are normally low; therefore, if smoothed EVI values <= 0.1, these water-related pixels are set as the fully inundated

pixels. If the smoothed EVI values > 0.1 and <= 0.3, then these water-related pixels are marked as the mixed pixels. The accuracy of the MODIS-derived surface water extent maps was estimated in Reference [47] by comparison with inundated maps provided by the Mekong River Commission (MRC) and with Landsat-derived inundated maps at the 10 km grid level (derived from the Normalized Difference Water Index (NDWI) with a threshold of 0.8). Results showed good agreement between three different inundation products. However, the MODIS-derived inundated area tends to be overestimated compared to results derived from MRC products, but inundated areas in flooded forests/marsh regions were considerably underestimated between August and September. This is related to the inability of optical sensors to look through vegetation canopy. In addition, MODIS-derived products showed an overestimation of surface-water extent in grids where Landsat-derived inundated area is >50 km^2. In contrast, MODIS-derived products showed an underestimation of surface water extent in grids where the Landsat-derived inundated area is <50 km^2. This problem is related to the difficulty to detect small water bodies from moderate resolution MODIS sensors. Based on these comparisons, it is concluded that there is a fundamental overestimation of MODIS-derived inundation products, but it can be used to roughly estimate the inundated areas at the scale of the LMB. The best feature of the MODIS products is their ability to provide continuously observations at both regional and global scales at high temporal resolution. This is very important to monitoring applications using satellite remote-sensing data.

3.2. Surface-Water Level Mapping

3.2.1. Construction of the Network of Altimetry Virtual Stations

Radar altimetry data are now commonly used for land hydrology (see Reference [48] for a recent review on the use of radar altimetry for hydrological applications). In the LMB in Vietnam and Cambodia, 45 virtual stations (VSs) were defined at the cross-section of ENVISAT altimetry ground tracks and inland water bodies (see Figure 1–right for their locations). The time series of water levels based on the ICE-1 retracked ranges [49] which provide accurate estimate of the height of the water bodies (e.g., Reference [50]), were derived using the Multimission Altimetry Processing Software (MAPS; see Reference [51] for details on the processing of the altimetry data) that is commonly used for this purpose (e.g., References [36,52–54]). Since the revisiting time of the ENVISAT is 35 days, there are only 11 values in one year at each VS. Although altimetry data provide instantaneous measurements over the area, we assume that water dynamics for such a big river basin is quite smooth, and results derived from instantaneous measurements are not far from the monthly mean values. Then, missing values are filled using the simple weight-smoothing function to build the monthly time series of surface-water level for the 2003–2009 period.

3.2.2. Interpolated Surface-Water Level Maps

Monthly maps of surface-water level of the study area can be estimated by combining monthly satellite altimetry data at all 45 ENVISAT VSs and MODIS-derived inundated maps. At a given month, satellite altimetry data at the VSs are linearly interpolated over the inundated areas (from the corresponding MODIS-derived surface water extent map described in Section 3.1) to estimate the surface-water level at each grid point of 500 m spatial resolution following the approach developed by Frappart et al. (2006) [33], and applied to MODIS-based inundation products [34,35]. Monthly maps of surface-water level of the study area at 500 m spatial resolution can be constructed for the 2003–2009 period.

3.3. Water-Volume Variations

3.3.1. Surface-Water Volume Variations

The variation of surface-water volume in the study area corresponds to the difference of surface-water levels integrated over the monthly MODIS-derived inundated areas. In References [18,30,40], the variation $\delta V(t_i,t_{i-1})$, between two consecutive months numbered i and $i-1$, over floodplain S, are the sum of the products of the difference of surface-water levels $\delta h_j(i, i-1)$ with $j = 1, 2, \ldots$ inside S, by the elementary surfaces $R_e^2\, sin(\theta j)\, \delta\theta\, \delta\lambda$ and the percentage of inundation P_j:

$$\delta V(i, i-1) = R_e^2 \delta\lambda \delta\theta \sum_{j \in S} P_j \delta h_j(\theta, \lambda, i, i-1) sin(\theta_j) \quad (4)$$

where $\delta\lambda$ and $\delta\theta$ are the sampling grid steps along longitude λ and latitude θ (0.0045°), respectively, and R_e is the mean radius of the Earth (6378 km). Surface-water volume variations are expressed in km^3/month. For the percentage of inundation P_j, we take 100% for water pixels, and 25% for mixed pixels.

3.3.2. Subsurface-Water Volume Variations

By definition, the time variations of total water storage (TWS) are the sum of the contribution of SWS, the soil moisture and the groundwater (see Equation (5)). Therefore, the variations of soil moisture and groundwater (called SSWS) can be estimated by calculating the difference between the TWS and the SWS:

$$\Delta TWS = \Delta SWS + \Delta SSWS \quad (5)$$

where the spatial–temporal variation of the TWS is measured using GRACE data, and the variation of the SWS is estimated using Equation (4) [18,26]. Similar to SWS, TWS and SSWS are generally expressed in km^3/month.

4. Results and Discussion

4.1. Monthly MODIS-Derived Land Surface-Water Extent Maps

Examples of monthly MODIS-derived land surface-water extent maps at 500 m spatial resolution within the study area (in January, April, July, and October 2003) are shown in Figure 2. Large water bodies (lakes and rivers) are clearly detected using MODIS imagery. In dry seasons, inundated areas are limited, and the surface-water extent reduces to its minimum stage, normally between March and April. Surface water starts to increase its extent when rainy seasons come in July and August, and reach maximum stage in October.

All available MOD09A1 observations over the 2003–2009 period are processed to obtain monthly time series of the surface-water extent within the study area during seven years, as shown in Figure 3 (blue curve). The variation of surface-water extent remains stable during the study period and ranges from ~6500 km^2 (low water stage) to ~40,000 km^2 (high water stage), without the occurrence of any large extreme hydrological event during 2003–2009. The maximum water extent in rainy seasons was observed in 2006 and 2007, while the minimum water extent was observed in 2003. One can note however that, during low water stages, the extent during 2006–2009 was slightly larger that during 2003–2005 (~15%) The variation of the surface-water extent is in good agreement with the variation of the in situ water level at the Tan Chau station (red curve), for a five-year period from 2003 to 2007, with a linear temporal correlation of 96%. This high correlation value confirms that MODIS-derived surface-water extent restitutes well the seasonal cycle of surface hydrology in this region.

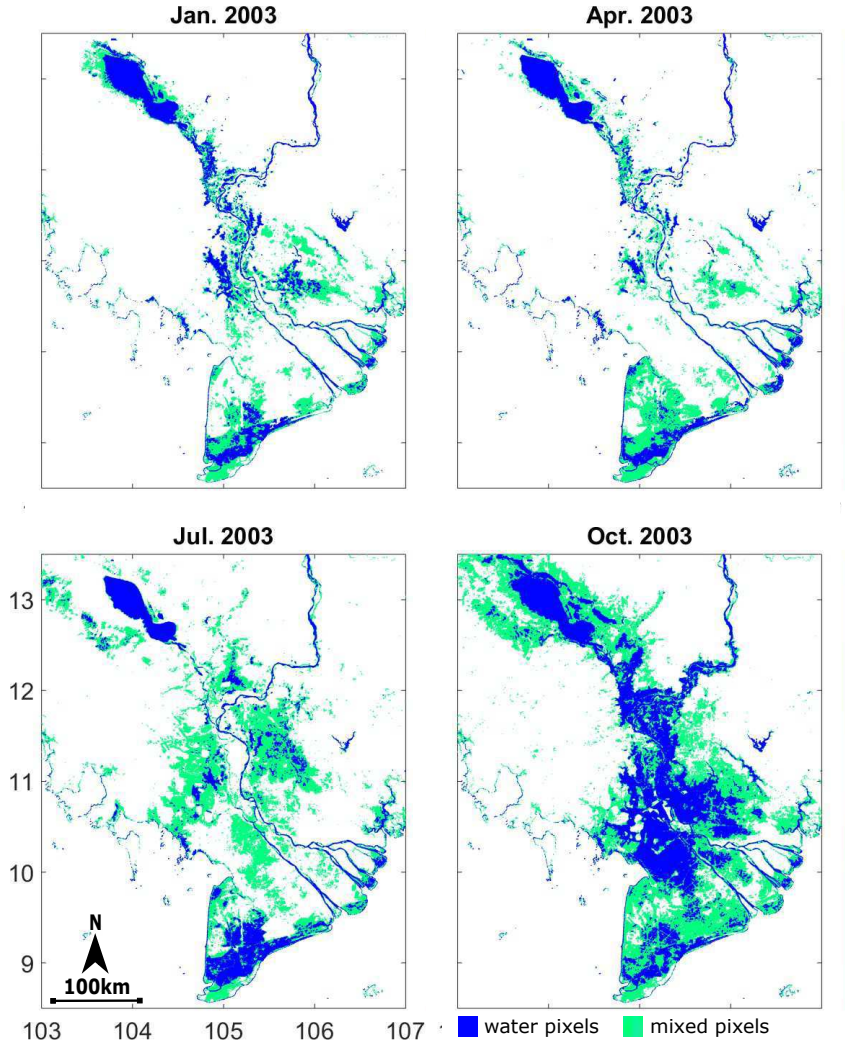

Figure 2. Examples of monthly MODIS-derived surface-water extent maps at 500 m spatial resolution within the study area in January, April, July, and October 2003, respectively, after applying the classification described in Reference [47]. For definition: Water pixels are totally inundated, while mixed pixels are partly inundated, and the inundation ratio is unknown. We assumed that 25% area of mixed pixels was inundated.

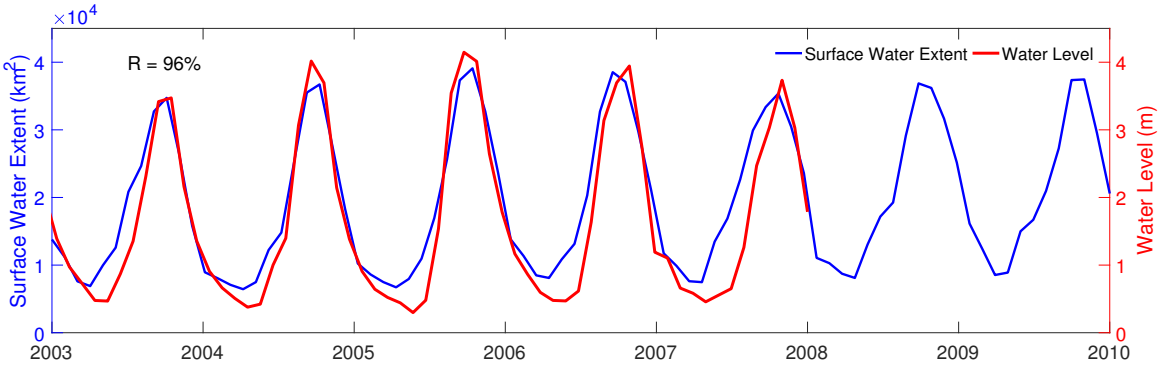

Figure 3. Blue: monthly time series of the surface-water extent of the study area (area shown in Figure 2), for the 2003–2009 period, after applying the classification described in Reference [47]. Red: monthly time series of water level at the Tan Chau station for the 2003–2007 period.

4.2. ENVISAT Altimetry and Surface Water Level Maps

4.2.1. ENVISAT Satellite-Based Surface Water Level

A representative selection (16 over 45) of the time series of surface-water levels at ENVISAT VSs are presented in Figure 4 (see locations of these 16 VSs in Figure 1-right). These VSs were selected so that their locations were representative of different parts of the study area. VSs 1–6 are located in the VMD, at the two main branches of the Mekong River in Vietnam. VSs 7–9 are located in the floodplains in between Vietnam and Cambodia, where the water-level variations are quite flat. VS 10 is located on the main stream of the river, showing a higher amplitude of the water level. VSs 11–16 are located in the upper part, on the Tonle Sap Lake where the seasonality is strong, with a mean annual amplitude of water level in the range of 5–7 m.

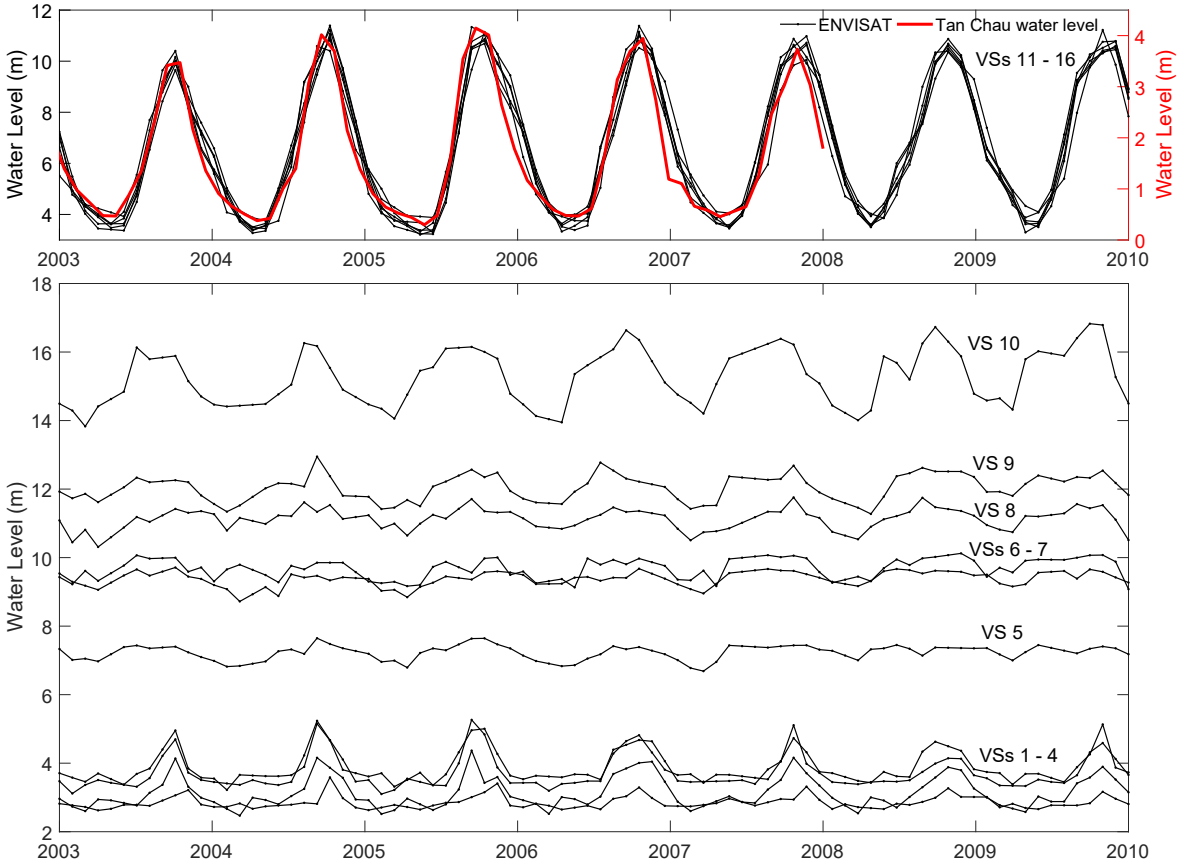

Figure 4. (**Top**) Monthly time series of surface-water level derived from ENVISAT altimetry data at VSs 11–16 located in the Tonle Sap Lake for the 2003–2009 period (black), and monthly time series of in situ water level at Tan Chau gauge station for the 2003–2007 period (red). (**Bottom**) Monthly time series of surface-water level derived from ENVISAT altimetry data at VSs 1–10 for the 2003–2009 period. Locations of these 16 VSs are shown in Figure 1-right.

For validation, the variation of the satellite-based water level at VS 14, located in the middle of the Tonle Sap Lake (12.40° N, 104.20° E), was compared to the variation of the in situ water level at the Tan Chau station for the 2003–2007 period (Figure 4-top panel). As expected, a high linear correlation of 92% was found between the two independent datasets. Comparisons between the same satellite-based water level and in situ water level (provided by the MRC) at other VSs in the LMB for the 2008–2016 period can be found in Reference [3], where they showed very good agreements between the two datasets. In addition, a high linear correlation of 92% was also found when comparing time series of the MODIS-derived surface-water extent (Figure 3) and time series of surface-water level at

VS 14 (Figure 4) over the common period (2003–2009). This high correlation confirms the consistency between these two highly related components. MODIS-derived surface water extent normally reaches its maximum levels at the same time as the maximum surface-water level of the Tonle Sap Lake, but its minimum levels occur before that of the surface-water level of the Lake. This is consistent with the fact that, during rainy seasons (June–October), the floodwater of the LMB flows directly into the Tonle Sap Lake through the Tonle Sap River; then, the Tonle Sap Lake stores and slowly releases water back to the VMD during dry seasons (November–May) [55].

4.2.2. Surface-Water Level Maps

As described in Section 3.2.2, maps of surface-water level are produced by applying linear interpolation on satellite-derived water level data. Examples of surface water level maps in the study area using water levels at 45 ENVISAT VSs are shown in Figure 5. The seasonal evolution for the period January to October 2003, covering a full rainy season period, exhibits very realistic spatial patterns with increasing water levels in July (up to 4–5 m) to reach their maximum values in October in the lower part of the delta, similar to what is observed in the in situ gauge records. From October (not shown), water levels start to decline, responding to the end of the rainy season.

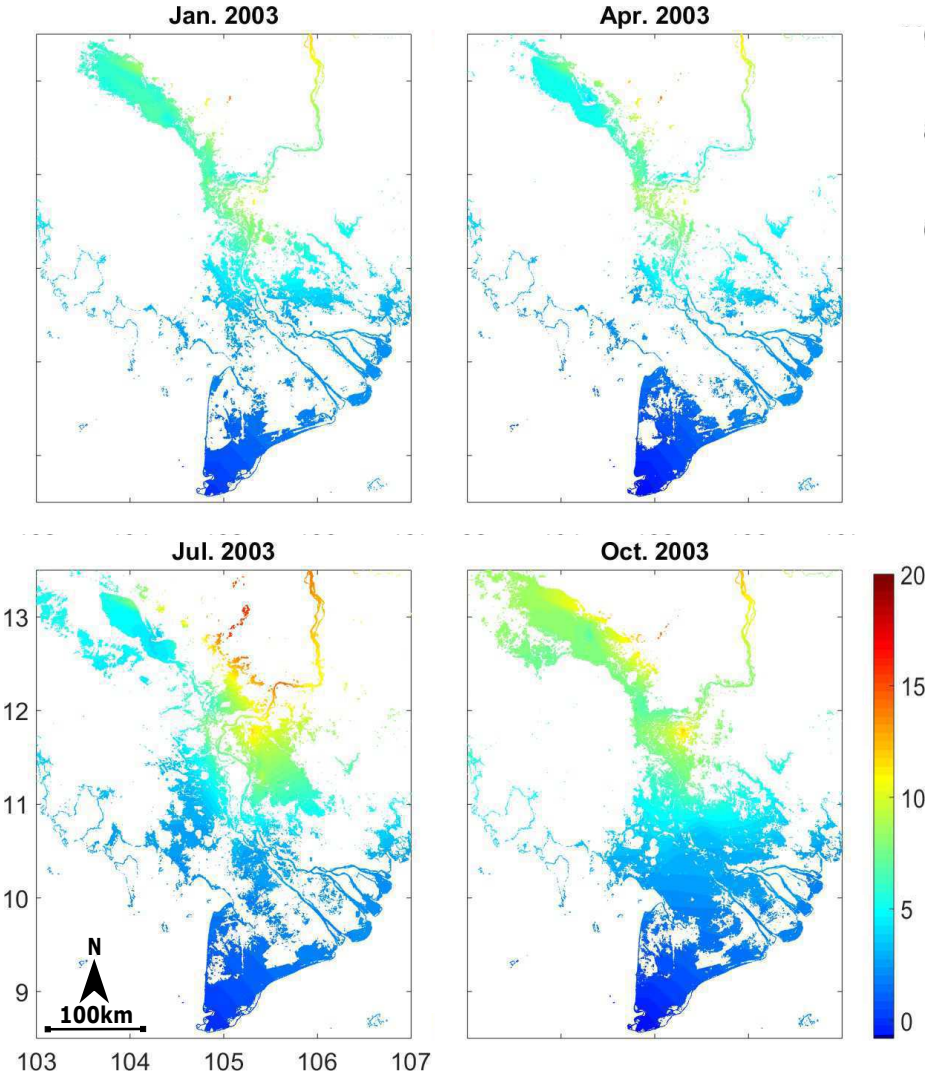

Figure 5. Altimetry-based surface water level maps (in m) within the study area in January, April, July, and October 2003, respectively. Linear interpolation based on ENVISAT altimetry data at 45 VSs is applied to produce monthly maps of surface water level at 500 m spatial resolution.

4.3. Surface and Subsurface Water Volume Variations

Monthly variation of SWS within the study area for the 2003–2009 period is shown in Figure 6. A strong seasonal cycle is evident with a mean annual amplitude of SWS of ∼39 km^3 (Figure 6). SWS gradually builds from January, with a larger increase from June to reach a maximum value observed in August–September. SWS starts to decrease from September to reach its minimum value in December. Given the absence of other independent, large-scale, multiyear SWS estimates over the LMB basin, the variability of our results over 2003–2009 is evaluated by comparison to the Mekong River discharge at the Tan Chau (10.48° N, 105.13° E) and Chau Doc (10.42° N, 105.06° E) stations. The sum of discharge at the two stations (Figure 6) is almost equal to the total discharge of the Mekong River when it flows from Cambodia to Vietnam. A very high linear temporal correlation is observed (96%) when comparing these two datasets during a seven-year period, as expected. Low and high peaks of these two components agree very well for all the study period. The mean annual amplitude of SWS in the study area amounts to ∼21% of the total volume of water that flows out of the Mekong River annually. Disaggregation of GRACE-derived TWS into satellite-derived SSWS variations is then carried out following Equation (5) and using the new SWS estimates. Monthly estimates of water storage in the three different hydrological reservoirs are computed for the entire period and are shown in Figure 7. Firstly, it compares monthly variation of SWS to the variations of TWS derived from GRACE data. A linear temporal correlation of 95% is observed that concludes to a similar dynamics and seasonal variations from peak to peak between the two parameters during the 2003–2009 period, with positive variations observed from May to October and negative variations between November and April. A one-month lag between SWS and TWS annual peak is evidenced (Figure 7), and this delay could be due to the exchange of water from the surface reservoir to the subsurface/groundwater reservoir and by the slower subsurface/groundwater flow in comparison to the surface water movement. Figure 7 also displays for the first time the estimations of monthly variation of SSWS within the LMB located in Vietnam and Cambodia. In agreement with the results of TWS and SWS changes, SSWS also shows a strong seasonal cycle, and its annual variation is ∼50 km^3, that corresponds to 55–60% of the total variation of the TWS, with a peak value also observed in September. SWS and SSWS outputs from the WGHM model (black and red, respectively) are also compared with our results. From the WGHM model, it is estimated that contribution of SWS and SSWS to the TWS over the study area is almost equal. Although good linear temporal correlations (>85%) are observed, the amplitudes of the SWS and SSWS from the WGHM are much smaller than our estimates (annual variation of ∼10 km^3 as compared to ∼40 km^3). This difference highlights the fact that large-scale hydrological modeling does not usually represent surface-water reservoirs (floodplains, reservoirs, delta) well enough, limiting the accurate estimates of SWS variations at regional to basin scale. Our results can help for future improvements of LMB modeling outputs, which are important for hydrological studies and water-resource management.

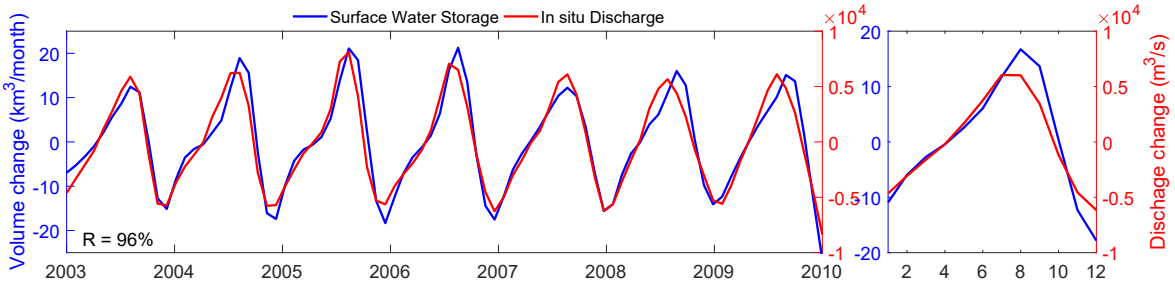

Figure 6. Monthly variation of the surface-water volume within the study area from our estimation (blue) for the 2003–2009 period. Monthly variations of the river discharge at Tan Chau and Chau Doc stations at the same period (red) are plotted for comparison.

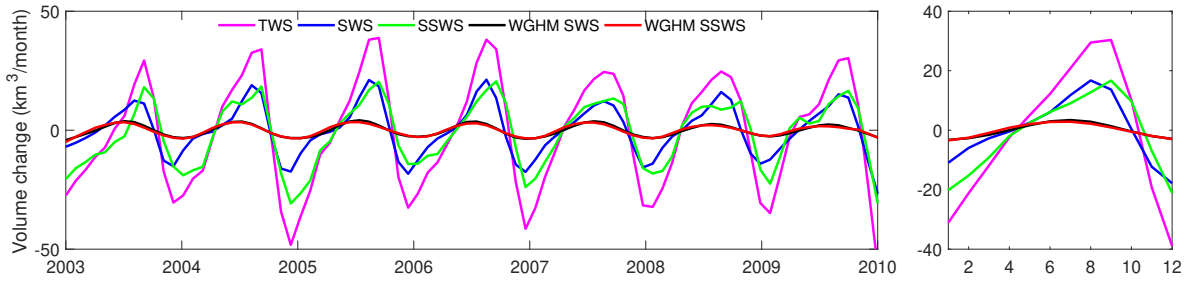

Figure 7. Comparison between the variations of SWS (blue) and SSWS (green) from our estimation with that derived from the WGHM model (black and red, respectively), and with variations of the total land surface-water storage derived from GRACE data (pink) for the 2003–2009 period.

Individual contribution of annual SWS and SSWS variations to TWS changes for the 2003–2009 period is shown in Figure 8-top. It shows that, for most of the years, variation of SWS is usually slightly lower than that of SSWS, except for 2006 and 2008, when SWS contribution dominates TWS variations. On the other hand, 2007 displays the largest difference between variations of SWS and SSWS, with SSWS contribution being ∼20% higher than SWS variations. Figure 8-bottom compares annual amplitude of TWS to annual cumulative precipitation of the Mekong basin derived from the gauge-calibrated Tropical Rainfall Measuring Mission Multisatellite Precipitation Analysis (TRMM/TMPA, 3B42 V7). Although rainfall in the Mekong basin was stable during the 2003–2009 period, TWS amplitude showed more variations, especially in 2007 and 2008, when it showed a negative anomaly compared to other years. This suggests that rainfall is not the only factor that drives the variations of water storage within the LMB and that other contributors, such as evapotranspiration and the impacts of human activities (water usage, dams, agriculture) might be at play. This needs more investigations in the future. This year-to-year variability highlights the importance to better understand the individual contribution of each of those reservoirs, and calls for future studies to investigate how they interact with each other and how they respond to climate variability, which still remain poorly known at a large scale. In particular, extracting the variation of the SSWS within the LMB is very important, as regular monitoring of groundwater has many potential applications. Knowing the variation of groundwater in the LMB is necessary because groundwater is the main source of drinking water in rural regions in Thailand, and especially in Cambodia, where >50% of the total drinking water comes from groundwater during the dry season [56,57]. It is predicted that the demand for freshwater will steadily increase in coming years due to the ongoing economic growth of countries in the LMB [16]. As surface water is often polluted or saline, using groundwater is still the main solution to satisfy this increasing freshwater demand [11]. Groundwater is also important for industrial and agricultural activities in the LMB, such as coffee plantations in the highlands of eastern Cambodia and mountainous regions of Laos, and rice and other crops production in the VMD where the delta provides food security for over 200 million people [7,16]. Groundwater, among other factors, is one of the key parameters to understand the impact of dam construction along the Mekong River to the water storage, agriculture, fisheries, biodiversity, and the ecosystem of the LMB [7,58,59]. For this purpose, our SWS and SSWS time series need to be extended for a longer period. As the VMD and its megacities (Ho Chi Minh City, for example) are facing high subsidence rates (current average subsidence rates are estimated at 1.1 cm year^{-1}, with areas over 2.5 cm year^{-1} [16]), regularly monitoring groundwater in the region is very important: groundwater overextraction in the VMD has been suggested as the main driver causing subsidence of the delta [14,15], as indicated by both the 3D hydrological model and InSAR-measured subsidence [16]. With extended time series of SWS and SSWS, we expect to obtain tools to investigate important socioeconomic and water-management political issues.

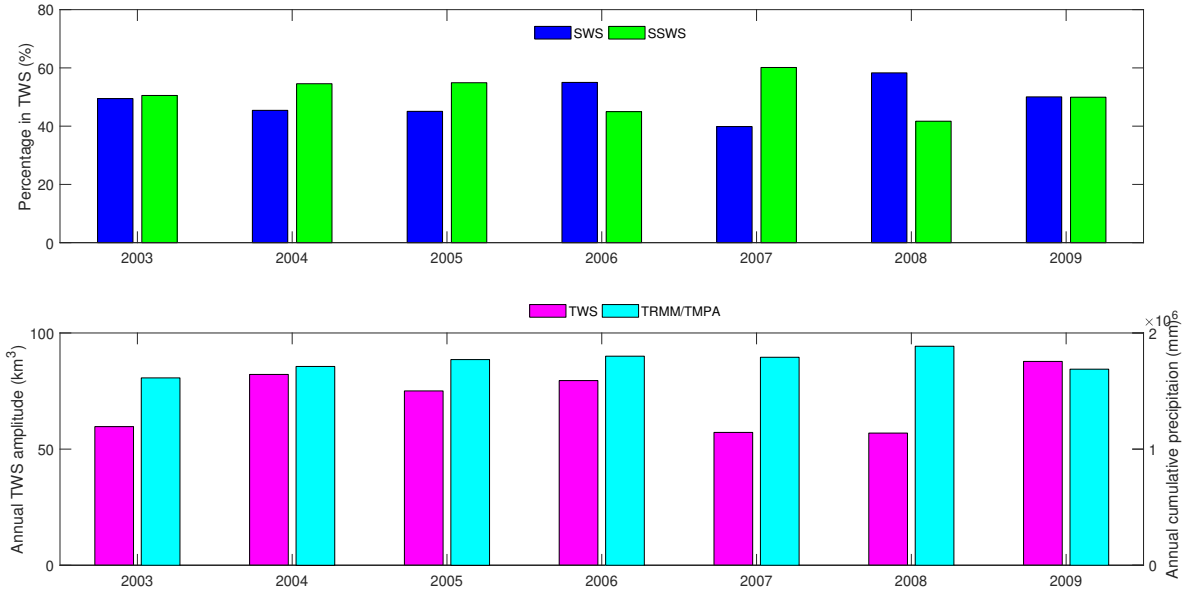

Figure 8. Top: Annual contribution (in %) of SWS and SSWS to TWS variation over the study area for the 2003–2009 period. Bottom: Annual amplitude of TWS of the study area, and annual cumulative rainfall of the Mekong basin for the 2003–2009 period.

5. Conclusions and Perspectives

In this study, monthly variation of SWS within the LMB (located in Cambodia and Vietnam) was estimated for the first time during the 2003–2009 period by combining MODIS imagery and ENVISAT altimetry data. MODIS atmospherically corrected land-surface reflectance eight-day Level 3 products (MOD09A1) were used to create monthly surface-water extent maps at 500 m spatial resolution in the study area, mainly based on the methodology introduced in Reference [47]. ENVISAT altimetry data at 45 satellite VSs were used to estimate monthly variation of the surface-water height at these locations. Then, linear interpolation was applied to estimate monthly surface-water height maps at similar spatial and temporal resolution as MODIS-derived surface-water extent maps. Finally, monthly variation of the SWS in the region was estimated as the product of the variations of the surface-water extent and surface-water height, following the approach described in References [18,30,35,40]. The variation of the SWS was validated by comparing with the variation of in situ discharge of the Mekong River and the variation of the TWS derived from GRACE data, showing very high linear temporal correlation of 96%, and 95%, respectively. Monthly variation of the SSWS of the region was also estimated for the first time by removing the variation of the SWS from the variation of the of TWS. Results showed that the variation of the SSWS corresponds to 55–60% of the variation of the TWS of the LMB located in Vietnam and Cambodia. Results from this study could also be used to improve hydrological models (e.g., the WGHM) at a regional scale. Extension of this product from 1995 until the present time requires to use longer time series of inundation maps, water level, and TWS. Long-term inundation maps can be obtained, for instance, from GIEMS [28,29] or GIEMS-D3 [60] datasets from multisource observations, or from the Landsat instrument [61]. Water levels can be obtained from other altimetry missions, e.g., European Remote-Sensing Satellite-2 (ERS-2, 1995–2003), SARAL (2013–2016), and Sentinel-3A and -3B (in operation since 2016 and 2018). Since GRACE mission data are only available from 2003, an attempt could be done to estimate the TWS from indirect measurements. Such an approach was used, for instance, in Reference [62] to extend back in time the GRACE data over the Mississippi basin using: (1) terrestrial water-cycle budget closure, and (2) precipitation, evapotranspiration, and runoff measurements. This approach can be extended to the global scale [63], and current efforts are focusing on the Asian region. Other GRACE solutions (like the global mascons solutions from JPL, GSFC, or CSR) could be evaluated to investigate the sensibility of our results to these different solutions. With the successful launch of the GRACE-FO, the successor of GRACE, on 22 May 2018, monthly

variation of TWS will be provided again soon. From these three longer time series, we should improve our understanding of climate variability and anthropogenic influences on SWS.

Author Contributions: Conceptualization, B.P.-D., C.P., and F.A.; data curation, B.P.-D. and S.B.; formal analysis, B.P.-D., F.P., C.P., and F.A.; investigation, B.P.-D., F.P.; methodology, B.P.-D., F.P., S.B., and F.F.; software, B.P.-D., S.B., and F.F.; supervision, C.P. and F.A.; validation, S.B. and F.F.; writing—original draft, B.P.-D., F.P., and F.F.; writing—review and editing, B.P.-D. and F.P. All authors contributed to the discussion of results and the preparation of the manuscript.

Funding: This study was financially supported by a PhD fellowship from the Vietnam International Education Development (911 project).

Acknowledgments: We acknowledge the data producers (NASA, ESA, CTOH/LEGOS, Goethe University Frankfurt, and VSRHC) for providing all datasets used in this study. We thank Nicolas Glatiot for the interesting discussions and suggestions during the preparation of the final manuscript. We would like to thank the three anonymous reviewers for their helpful comments and suggestions for improving the quality of our manuscript.

Conflicts of Interest: The authors declare no conflict of interest. The founding sponsor had no role in the design of the study; in the collection, analyses, and interpretation of data; in the writing of the manuscript; and in the decision to publish the results.

References

1. Mekong River Commission. *Planning Atlas of the Lower Mekong River Basin, Basic Development Plan Programme for Sustainable Development*; Technical Report; Mekong River Commission: Phnom Penh, Cambodia, 2011.
2. Hori, H. *The Mekong Environment and Development*; United Nations University: New York, NY, USA, 2000.
3. Pham-Duc, B. Satellite Remote Sensing of the Variability of the Continental Hydrology Cycle in the Lower Mekong Basin over the Last Two Decades. Ph.D. Thesis, Sorbonne Université, Paris, France, 2018.
4. Le, A.T.; Chinvanno, S. Climate Change in the Mekong River Delta and Key Concerns on Future Climate Threats. *Adv. Glob. Chang. Res.* **2011**, *45*. [CrossRef]
5. Pham-Duc, B.; Prigent, C.; Aires, F. Surface Water Monitoring within Cambodia and the Vietnamese Mekong Delta over a Year, with Sentinel-1 SAR Observations. *Water* **2017**, *9*, 366. [CrossRef]
6. Pech, S.; Sunada, K. Population Growth and Natural-Resources Pressures in the Mekong River Basin. *Ambio* **2008**, *37*, 219–224. [CrossRef]
7. Pokhrel, Y.; Burbano, M.; Roush, J.; Kang, H.; Sridhar, V.; Hyndman, D.W. A Review of the Integrated Effects of Changing Climate, Land Use, and Dams on Mekong River Hydrology. *Water* **2018**, *10*, 266. [CrossRef]
8. FAO. *El Niño Event in Viet Nam*; Food and Agriculture Organization of the United Nations: Rome, Italy, 2016.
9. Giri, C.; Defourny, P.; Shrestha, S. Land cover characterization and mapping of continental Southeast Asia using multi-resolution satellite sensor data. *Int. J. Remote Sens.* **2003**, *24*, 4181–4196. [CrossRef]
10. Tran, H.; Tran, T.; Kervyn, M. Dynamics of Land Cover/Land Use Changes in the Mekong Delta, 1973–2011: A Remote Sensing Analysis of the Tran Van Thoi District, Ca Mau Province, Vietnam. *Remote Sens.* **2015**, *7*, 2899–2925. [CrossRef]
11. Wagner, F.; Tran, V.B.; Renaud, F.G. Groundwater Resources in the Mekong Delta: Availability, Utilization and Risks. In *The Mekong Delta System: Interdisciplinary Analyses of a River Delta*; Renaud, F.G., Kuenzer, C., Eds.; Springer: Dordrecht, The Netherlands, 2012; pp. 201–220. [CrossRef]
12. Minderhoud, P.S.J.; Coumou, L.; Erban, L.E.; Middelkoop, H.; Stouthamer, E.; Addink, E.A. The relation between land use and subsidence in the Vietnamese Mekong delta. *Sci. Total Environ.* **2018**, *634*, 715–726. [CrossRef]
13. Galloway, D.L.; Burbey, T.J. Review: Regional land subsidence accompanying groundwater extraction. *Hydrogeol. J.* **2011**, *19*, 1459–1486. [CrossRef]
14. Erban, L.E.; Gorelick, S.M.; Zebker, H.A.; Fendorf, S. Release of arsenic to deep groundwater in the Mekong Delta, Vietnam, linked to pumping-induced land subsidence. *Proc. Natl. Acad. Sci. USA* **2013**, *110*, 13751–13756. [CrossRef]
15. Erban, L.E.; Gorelick, S.M.; Zebker, H.A. Groundwater extraction, land subsidence, and sea-level rise in the Mekong Delta, Vietnam. *Environ. Res. Lett.* **2014**, *9*, 084010. [CrossRef]

16. Minderhoud, P.S.J.; Erkens, G.; Pham, V.H.; Bui, V.T.; Erban, L.; Kooi, H.; Stouthamer, E. Impacts of 25 years of groundwater extraction on subsidence in the Mekong delta, Vietnam. *Environ. Res. Lett.* **2017**, *12*, 064006. [CrossRef] [PubMed]
17. Rodell, M.; Famiglietti, J.S.; Wiese, D.N.; Reager, J.T.; Beaudoing, H.K.; Landerer, F.W.; Lo, M.H. Emerging trends in global freshwater availability. *Nature* **2018**, 651–659. [CrossRef] [PubMed]
18. Frappart, F.; Papa, F.; Güntner, A.; Werth, S.; Santos, J.; Tomasella, J.; Seyler, F.; Prigent, C.; Rossow, W.B.; Calmant, S.; et al. Satellite-based estimates of groundwater storage variations in large drainage basins with extensive floodplains. *Remote Sens. Environ.* **2011**, *115*, 1588–1594. [CrossRef]
19. Shamsudduha, M.; Taylor, R.G.; Longuevergne, L. Monitoring groundwater storage changes in the highly seasonal humid tropics: Validation of GRACE measurements in the Bengal Basin. *Water Resour. Res.* **2012**, *48*. [CrossRef]
20. Becker, M.; Papa, F.; Frappart, F.; Alsdorf, D.; Calmant, S.; Da Silva, J.S.; Prigent, C.; Seyler, F. Satellite-based estimates of surface water dynamics in the Congo River Basin. *Int. J. Appl. Earth Obs. Geoinf.* **2018**, 196–209. [CrossRef]
21. Khaki, M.; Forootan, E.; Kuhn, M.; Awange, J.; Papa, F.; Shum, C.K. A study of Bangladesh's sub-surface water storages using satellite products and data assimilation scheme. *Sci. Total Environ.* **2018**, 963–977. [CrossRef]
22. Frappart, F.; Ramillien, G. Monitoring Groundwater Storage Changes Using the Gravity Recovery and Climate Experiment (GRACE) Satellite Mission: A Review. *Remote Sens.* **2018**, *10*. [CrossRef]
23. Singh, A.; Behrangi, A.; Fisher, J.B.; Reager, J.T. On the Desiccation of the South Aral Sea Observed from Spaceborne Missions. *Remote Sens.* **2018**, *10*, 793. [CrossRef]
24. Zhang, Z.; Chang, J.; Xu, C.Y.; Zhou, Y.; Wu, Y.; Chen, X.; Jiang, S.; Duan, Z. The response of lake area and vegetation cover variations to climate change over the Qinghai-Tibetan Plateau during the past 30 years. *Sci. Total Environ.* **2018**, *635*, 443–451. [CrossRef] [PubMed]
25. Singh, A.; Kumar, U.; Seitz, F. Remote Sensing of Storage Fluctuations of Poorly Gauged Reservoirs and State Space Model (SSM)-Based Estimation. *Remote Sens.* **2015**, *7*, 17113–17134. [CrossRef]
26. Papa, F.; Frappart, F.; Malbeteau, Y.; Shamsudduha, M.; Vuruputur, V.; Sekhar, M.; Ramillien, G.; Prigent, C.; Aires, F.; Pandey, R.K.; et al. Satellite-derived surface and sub-surface water storage in the Ganges-Brahmaputra River Basin. *J. Hydrol. Reg. Stud.* **2015**, *4*, 15–35. [CrossRef]
27. Prigent, C.; Matthews, E.; Aires, F.; Rossow, W.B. Remote sensing of global wetland dynamics with multiple satellite data sets. *Geophys. Res. Lett.* **2001**, *28*, 4631–4634. [CrossRef]
28. Prigent, C.; Papa, F.; Aires, F.; Rossow, W.B.; Matthews, E. Global inundation dynamics inferred from multiple satellite observations, 1993-2000. *J. Geophys. Res. Atmos.* **2007**, *112*, 1–13. [CrossRef]
29. Prigent, C.; Papa, F.; Aires, F.; Jimenez, C.; Rossow, W.B.; Matthews, E. Changes in land surface water dynamics since the 1990s and relation to population pressure. *Geophys. Res. Lett.* **2012**, *39*, L08403. [CrossRef]
30. Frappart, F.; Papa, F.; Famiglietti, J.S.; Prigent, C.; Rossow, W.B. Interannual variations of river water storage from a multiple satellite approach: A case study for the Rio Negro River basin. *J. Geophys. Res.* **2008**, *113*, 1–12. [CrossRef]
31. Frappart, F.; Papa, F.; Guuntner, A.; Werth, S.; Ramillien, G.; Prigent, C.; Rossow, W.B.; Bonnet, M.P. Interannual variations of the terrestrial water storage in the Lower Ob' Basin from a multisatellite approach. *Hydrol. Earth Syst. Sci.* **2010**, *14*, 2443–2453. [CrossRef]
32. Frappart, F.; Papa, F.; da Silva, J.S.; Ramillien, G.; Prigent, C.; Seyler, F.; Calmant, S. Surface freshwater storage and dynamics in the Amazon basin during the 2005 exceptional drought. *Environ. Res. Lett.* **2012**, *7*, 044010. [CrossRef]
33. Frappart, F.; Do Minh, K.; L'Hermitte, J.; Cazenave, A.; Ramillien, G.; Le Toan, T.; Mognard-Campbell, N. Water volume change in the lower Mekong from satellite altimetry and imagery data. *Geophys. J. Int.* **2006**, *167*, 570–584. [CrossRef]
34. Frappart, F.; Biancamaria, S.; Normandin, C.; Blarel, F.; Bourrel, L.; Aumont, M.; Azemar, P.; Vu, P.L.; Le Toan, T.; Lubac, B.; et al. Influence of recent climatic events on the surface water storage of the Tonle Sap Lake. *Sci. Total Environ.* **2018**, 1520–1533. [CrossRef] [PubMed]

35. Normandin, C.; Frappart, F.; Lubac, B.; Bélanger, S.; Marieu, V.; Blarel, F.; Robinet, A.; Guiastrennec-Faugas, L. Quantification of surface water volume changes in the Mackenzie Delta using satellite multi-mission data. *Hydrol. Earth Syst. Sci.* **2018**, *22*, 1543–1561. [CrossRef]
36. Biancamaria, S.; Frappart, F.; Leleu, A.S.; Marieu, V.; Blumstein, D.; Desjonquères, J.D.; Boy, F.; Sottolichio, A.; Valle-Levinson, A. Satellite radar altimetry water elevations performance over a 200 m wide river: Evaluation over the Garonne River. *Adv. Space Res.* **2017**, 128–146. [CrossRef]
37. Vermote, E. MOD09A1 MODIS Surface Reflectance 8-Day L3 Global 500m SIN Grid V006. *Nasa Eosdis Land Process. Daac* **2015**. [CrossRef]
38. Benveniste, J.; Roca, M.; Levrini, G.; Vincent, P.; Baker, S.; Zanife, O.; Zelli, C.; Bombaci, O. The Radar Altimetry Mission: RA-2, MWR, DORIS and LRR. *ESA Bull.* **2001**, *106*, 25101–25108.
39. Roux, E.; Santos, J.; Cesar, A.; Getirana, V.; Bonnet, M.P.; Calmant, S.; Martinez, J.M. Producing time series of river water height by means of satellite radar altimetry—A comparative study. *Hydrol. Sci. J.* **2010**, *55*, 104–120. [CrossRef]
40. Papa, F.; Frappart, F.; Güntner, A.; Prigent, C.; Aires, F.; Getirana, A.C.V.; Maurer, R. Surface freshwater storage and variability in the Amazon basin from multi-satellite observations, 1993–2007. *J. Geophys. Res. Atmos.* **2013**, *118*, 11951–11965. [CrossRef]
41. Wiese, D.N.; Landerer, F.W.; Watkins, M.M. Quantifying and reducing leakage errors in the JPL RL05M GRACE mascon solution. *Water Resour. Res.* **2016**, *52*, 7490–7502. [CrossRef]
42. Tapley, B.D.; Bettadpur, S.; Watkins, M.; Reigber, C. The gravity recovery and climate experiment: Mission overview and early results. *Geophys. Res. Lett.* **2004**, *31*, 1–4. [CrossRef]
43. Sakumura, C.; Bettadpur, S.; Bruinsma, S. Ensemble prediction and intercomparison analysis of GRACE time-variable gravity field models. *Geophys. Res. Lett.* **2014**, *41*, 1389–1397. [CrossRef]
44. Landerer, F.W.; Swenson, S.C. Accuracy of scaled GRACE terrestrial water storage estimates. *Water Resour. Res.* **2012**, *48*. [CrossRef]
45. Doll, P.; Kaspar, F.; Lehner, B. A global hydrological model for deriving water availability indicators: Model tuning and validation. *J. Hydrol.* **2003**, *270*, 105–134. [CrossRef]
46. Doll, P.; Muller Schmied, H.; Schuh, C.; Portmann, F.T.; Eicker, A. Global-scale assessment of groundwater depletion and related groundwater abstractions: Combining hydrological modeling with information from well observations and GRACE satellites. *Water Resour. Res.* **2014**, *50*, 5698–5720. [CrossRef]
47. Sakamoto, T.; van Nguyen, N.; Kotera, A.; Ohno, H.; Ishitsuka, N.; Yokozawa, M. Detecting temporal changes in the extent of annual flooding within the Cambodia and the Vietnamese Mekong Delta from MODIS time-series imagery. *Remote Sens. Environ.* **2007**, *109*, 295–313. [CrossRef]
48. Crétaux, J.F.; Nielsen, K.; Frappart, F.; Papa, F.; Calmant, S.; Benveniste, J. *Hydrological Applications of Satellite Altimetry: Rivers, Lakes, Man-Made Reservoirs, Inundated Areas*, earth obse ed.; CRC Press: Boca Raton, FL, USA, 2017; pp. 459–504.
49. Wingham, D.J.; Rapley, C.G.; Griffiths, H. New techniques in satellite altimeter tracking systems. In Proceedings of the 1986 International Geoscience and Remote Sensing Symposium(IGARSS'86) on Remote Sensing: Today's Solutions for Tomorrow's Information Needs, Zürich, Switzerland, 8–11 September 1986; Volume 3.
50. Frappart, F.; Calmant, S.; Cauhopé, M.; Seyler, F.; Cazenave, A. Preliminary results of ENVISAT RA-2-derived water levels validation over the Amazon basin. *Remote Sens. Environ.* **2006**, *100*, 252–264. [CrossRef]
51. Normandin, C.; Frappart, F.; Diepkile, A.T.; Marieu, V.; Mougin, E.; Blarel, F.; Lubac, B.; Braquet, N.; Ba, A. Evolution of the Performances of Radar Altimetry Missions from ERS-2 to Sentinel-3A over the Inner Niger Delta. *Remote Sens.* **2018**, *10*, 833. [CrossRef]
52. Frappart, F.; Papa, F.; Marieu, V.; Malbeteau, Y.; Jordy, F.; Calmant, S.; Durand, F.; Bala, S. Preliminary Assessment of SARAL/AltiKa Observations over the Ganges-Brahmaputra and Irrawaddy Rivers. *Mar. Geod.* **2015**, *38*, 568–580. [CrossRef]
53. Biancamaria, S.; Schaedele, T.; Blumstein, D.; Frappart, F.; Boy, F.; Desjonquères, J.D.; Pottier, C.; Blarel, F.; Niño, F. Validation of Jason-3 tracking modes over French rivers. *Remote Sens. Environ.* **2018**, *209*, 77–89. [CrossRef]

54. Bogning, S.; Frappart, F.; Blarel, F.; Niño, F.; Mahé, G.; Bricquet, J.P.; Seyler, F.; Onguéné, R.; Etamé, J.; Paiz, M.C.; et al. Monitoring Water Levels and Discharges Using Radar Altimetry in an Ungauged River Basin: The Case of the Ogooué. *Remote Sens.* **2018**, *10*, 350. [CrossRef]
55. Cochrane, T.A.; Arias, M.E.; Piman, T. Historical impact of water infrastructure on water levels of the Mekong River and the Tonle Sap system. *Hydrol. Earth Syst. Sci.* **2014**, *18*, 4529–4541. [CrossRef]
56. Ha, K.; Ngoc, N.T.M.; Lee, E.; Jayakumar, R. *Current Status and Issues of Groundwater in the Mekong River Basin*; Korea Institute of Geoscience and Mineral Resources (KIGAM): Bangkok, Thailand, 2015; p. 121.
57. Pokhrel, Y.N.; Felfelani, F.; Shin, S.; Yamada, T.J.; Satoh, Y. Modeling large-scale human alteration of land surface hydrology and climate. *Geosci. Lett.* **2017**, *4*, 10. [CrossRef]
58. Ziv, G.; Baran, E.; Nam, S.; Rodríguez-Iturbe, I.; Levin, S.A. Trading-off fish biodiversity, food security, and hydropower in the Mekong River Basin. *Proc. Natl. Acad. Sci. USA* **2012**, *109*, 5609–5614. [CrossRef]
59. Intralawan, A.; Wood, D.; Frankel, R. *Economic Evaluation of Hydropower Projects in the Lower Mekong Basin*; Mae Fah Luang University: Chiang Rai, Thailand, 2017; p. 21.
60. Aires, F.; Miolane, L.; Prigent, C.; Pham, B.; Fluet-Chouinard, E.; Lehner, B.; Papa, F. A Global Dynamic Long-Term Inundation Extent Dataset at High Spatial Resolution Derived through Downscaling of Satellite Observations. *J. Hydrometeorol.* **2017**, *18*, 1305–1325. [CrossRef]
61. Pekel, J.F.; Cottam, A.; Gorelick, N.; Belward, A.S. High-resolution mapping of global surface water and its long-term changes. *Nature* **2016**, *540*, 418–422. [CrossRef] [PubMed]
62. Munier, S.; Aires, F.; Schlaffer, S.; Prigent, C.; Papa, F.; Maisongrande, P.; Pan, M. Combining data sets of satellite-retrieved products for basin-scale water balance study: 2. Evaluation on the Mississippi Basin and closure correction model. *J. Geophys. Res. Atmos.* **2014**, *119*, 12100–12116. [CrossRef]
63. Aires, S.M.F. A new global method of satellite dataset merging and quality characterization constrained by the terrestrial water budget. *Remote Sens. Environ.* **2018**, *205*, 119–130. [CrossRef]